MODE SELECTION BEHAVIOR OF VHF THERMAL-PIEZORESISTIVE SELF-SUSTAINED OSCILLATORS

H.J. Hall[1]*, D.E. Walker[2], L. Wang[1], R.C. Fitch[2], J.S. Bunch[1], S. Pourkamali[3], and V.M. Bright[1]
[1]University of Colorado at Boulder, Boulder, CO, USA
[2]Air Force Research Laboratory, Wright-Patterson AFB, OH, USA
[3]University of Denver, Denver, CO

ABSTRACT

The work demonstrates performance of thermal-piezoresistive self-sustained oscillators in both vacuum and ambient air conditions, up to 161MHz with AC peak-to-peak voltages of up to 44mV. The devices are of an I-shaped geometry fabricated from 1.6-1.9μm thick n-type silicon. While strong resonance is demonstrated in their intended in-plane longitudinal structural mode (g_m up to -238 μA/V), the device oscillation was verified by laser vibration sensing to occur in a different mode. Finite element simulation suggests that the longitudinally symmetric flexural mode is the mode of oscillation.

KEYWORDS

Oscillator, Resonator, VHF, limit cycle oscillation

INTRODUCTION

Thermally-actuated piezoresistively readout resonant devices fabricated from single-crystal silicon have been recently demonstrated as viable alternatives to capacitive and piezoelectric systems for a variety of sensing applications. In addition, if fabricated from n-type silicon they offer the unique potential to exhibit self-sustained oscillation [1], [2] which affords operation as on-chip resonant sensors without the complications of integrated feedback circuitry or a coupled AC drive signal. Expanding their spectral range of operation would also increase their potential for direct use as oscillators in on-chip RF-electronics applications. To this end, this work expands upon previous efforts [3], [4] to increase both the operating frequency and performance of these devices by reducing the scaling of their geometry. Specifically, we have successfully demonstrated self-sustained oscillation in the VHF regime. However, the devices in this work operate in a different mode than previous work.

The devices presented are fabricated in a similar 2-terminal I-shaped geometry as previously reported, intended to operate in the in-plane longitudinal structural mode through cyclic Joule heating of the actuator arms. These devices differ in that they are fabricated from a thicker n-type SOI device layer with similar submicron geometry. This thickness was pursued with the intent of obtaining higher mechanical quality factor, Q_m, and allowing higher I_{DC} values to enhance the motional conductance at resonance ($\omega=\omega_o$), g_m, defined in [4] as

$$g_m = 2\alpha E\pi_l Q_m \frac{I_{DC}^2}{C_{th}\omega_o} \qquad (1)$$

where C_{th} is the effective thermal capacitance of the lumped actuator element, E is the Young's modulus, π_l is the longitudinal piezoresistive coefficient, and α is the coefficient of thermal expansion.

The self-sustained oscillation phenomena, described in [1], is the result of internal feedback within the device that is only possible when the piezoresistive coefficient is negative, as is the case for n-type silicon. The interaction between the thermal, mechanical and electrical subsystems of the devices creates the necessary closed loop gain and 360° phase shift needed for oscillation. The effective Q is describing this behavior is

$$Q_{eff} = \frac{Q_m}{1 + R_A g_m} \qquad (2)$$

where R_A is the physical electrical resistance of the device. When $g_m R_A \leq -1$, self-sustained oscillations can be initiated by the thermal noise present in the system.

FABRICATION

The devices presented in this work were fabricated on the same chip using a process similar to that previously reported in [3], with the following differences. First, the starting SOI wafer had a ~1.5μm thick device layer (n-type, ρ=0.1 Ω-cm), initially thinned by thermal oxidation, and a ~3μm thick buried oxide. Second, the submicron device patterning was performed using a direct write electron beam lithography (EBL) system across the entire chip using PMMA resist (~100 nm thick). Chromium (~145nm thick) alone was found to be sufficient for pattern alignment (no Au layer). Third, to accommodate the thicker Si device layer, the silicon etching was performed using a time multiplexed RIE system (PlasmaTherm Versaline VL-8526). Finally, thermal oxidation (dry, 1100 °C, 50 min) was performed prior to release to smooth the scalloping from the etch.

Post fabrication SEM images of Device A3 are shown in Figure 1. Some undercutting of the silicon is evident as is the traditional scalloping from time multiplexed DSE. Table 1 summarizes the dimensions of the two devices being reported in this work.
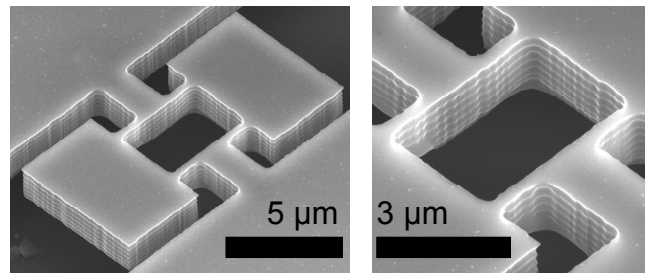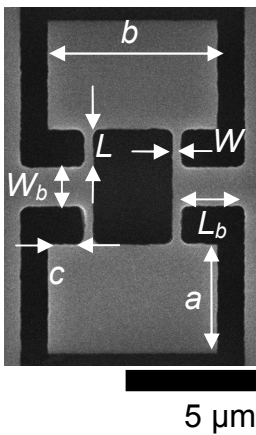

Figure 1: SEM image of Device A3 (45° tilted, oblique) with a close up of the actuator arms

Table 1: Top View of Device A3 with average device dimensions[n=7]in μm (h = device thickness)

| Device	A3	C6
h	1.6	1.77
a	6.46	5.73
b	4.17	5.70
c	1.38	0.94
L	1.47	2.02
W	0.36	0.34
W_b	1.54	1.59
L_b	2.56	2.56

5 μm

Figure 2: Sensing testbed (ambient air) used for sensing the spectral response of the structural mode while measuring electrical output of the device in self-sustained oscillation. (Position of laser shown on inset SEM image)

EXPERIMENTAL METHOD
Resonator Testing
Before testing as self-sustained oscillators, the devices were first examined as resonators to identify the electrical modes. This was accomplished using a network analyzer (Agilent E5061B ENA series) to measure the magnitude of the S_{21} parameter (device transmission) in both vacuum (50-70 Torr) and ambient air conditions. Frequency sweeps were conducted between 10-250 MHz to identify electrical modes, which were then individually examined over an incremental range of I_{DC} values. It was shown experimentally, that grounding the substrate had no effect on the output and thus the substrate was left ungrounded.

Self-Sustained Oscillator Testing
The device performance as self-sustained oscillators was initially examined both electrically using the test board circuit shown in Figure 2 (dashed outline). The AC voltage output was recorded in the time-domain using a digital oscilloscope (Agilent DSO7032A, DC coupled, 1MΩ input impedance). This testing was conducted in both vacuum and ambient air conditions over an incremental range of I_{DC} values.

Electrical measurements of resonators can at times be confused by mixing effects which can complicate identification of the structural mode in which the device is operating. To assist in this end a laser sensing testbed was employed while electrically operating the device in ambient air to identify the frequency of mechanical oscillation and observe its spectral response. Figure 4 describes the testbed which use a HeNe laser to illuminate the top edge of the upper device plate (spot size ~1μm). This laser reflects off of the underlying Si substrate and the device itself and the return is captured with a photodiode. Mechanical motion of the device structure modulates the intensity of the laser return at the frequency of self-sustained oscillation. The electrical output of the photodiode is then captured and recorded by a spectrum analyzer (Agilent 9320B).

RESULTS AND DISCUSSION
Electrical Resonant Modes
Both devices exhibited very similar electrical
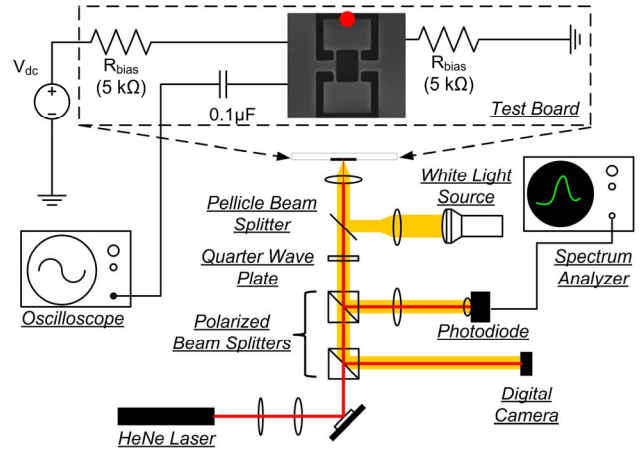
resonant responses. An overview of the measured S_{21} response for Device C6 is shown in Figure 3 (see caption for test conditions) with four resonant peaks observed. These four peaks are a result of driving the device electrically in two different structural resonant modes by different means. Examining the power applied to the lumped actuator resistance of the device, P_A, described by Eq (3) provides an explanation.

$$P_A = \frac{(V_{ac}\sin\omega t + V_{dc})^2}{R_A}$$

$$= \left[\frac{V_{ac}^2 + 2V_{dc}^2}{2R_A}\right] + \left[\frac{2V_{ac}V_{dc}\sin\omega t}{R_A}\right] - \left[\frac{V_{ac}^2\cos 2\omega t}{2R_A}\right] \tag{3}$$

The lower frequency peaks in Figure 3 are a result of AC excitation of the structural mode, which is described by the final term of (3) and previously reported in [5]. The middle term of (3) describes the conventional operation of the device which utilizes power from both the AC and DC sources. The higher frequency peaks are a result of this term and occur at the frequency of the structural mode. The initial term in (3) is DC power loss. The electrical resonant response of these devices was unexpected as previously reported work [3], [4] showed only operation in what was presumed to be the higher frequency in-plane longitudinal mode. This presumption was based upon the fact that this mode shape was the only one that offered the ability to both *actuate* the structural mode through AC thermal expansion of the actuator arms and *sense* the mode through the piezoresistive change occurring within them. Analysis of the structural modes using COMSOL (unstressed, room temp fixed Young's modulus), suggests that the $\omega_{o(\#2)}$ mode is the in-plane longitudinal mode previously reported, and that the $\omega_{o(\#1)}$ is a longitudinally symmetric flexural mode (see inset images in Figure 3). We believe the actuation of the flexural mode is attributed to slight non-uniformity of vertical profile in the actuator arms, creating a vertical AC temperature gradient.

Measured responses of each of these AC+DC modes for Device C6 are shown in Figure 4. Using the de-embedding procedure presented in [3], the *apparent Q* (i.e. background phase uncorrected) and g_m are listed for each. While the mechanical Q are likely lower than these
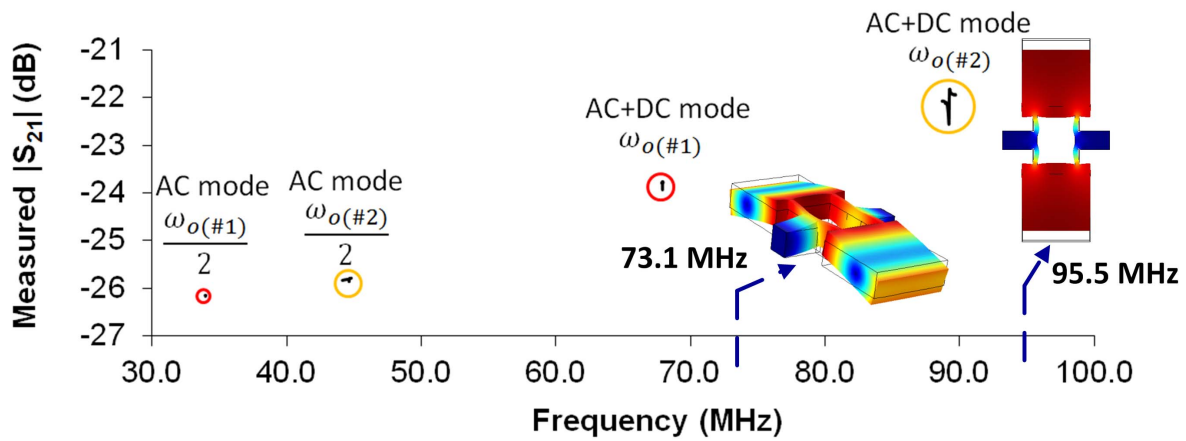
Figure 3: Measured $|S_{21}|$ data (vacuum) indicating position of resonant modes for Device C6. The AC mode data shown (~33.9MHz and 44.7MHz) was collected at +10dBm input power with I_{DC} 1.45mA and I_{DC} =0.747mA respectively. The AC+DC (~67.8 MHz and ~88.9MHz) were both collected at I_{DC} = 1.45mA with -30dBm input power. Inset are the two corresponding resonant structural mode shapes produced using COMSOL modal analysis (unstressed, Temp=285K, E=130 GPa) and their resonant frequencies. The 73.1 MHz mode shown is a longitudinally symmetric flexural mode, while the 95.5MHz mode shown is the in-plane longitudinal mode. Device A3 (not shown) exhibited a similar response with $f_{o(\#1)}$=~81.6MHz and $f_{o(\#2)}$=~105.6MHz although the corresponding AC mode at $f_{o(\#1)}/2$ was below the noise floor.

indicated values, the trend clearly indicates that self-Q enhancement, previously reported in [1], is occurring prior to self-sustained oscillation in the $\omega_{o(\#1)}$ mode. The amplitude of the $\omega_{o(\#2)}$ grows with I_{DC}, which is expected according to (1), however despite exhibiting stronger g_m values the self-Q enhancement effect does not occur.

Self-Sustained Oscillator Performance

Remarkably, at higher I_{DC} values, self-sustained oscillation was exhibited for both devices with mixed frequency content existing at $\omega_{o(\#1)}$ and its primary harmonic $2\omega_{o(\#1)}$. Applying a least-squares (LS) fit of the temporal data recorded to a dual sinusoidal function allows for direct estimation of the percentage of signal content, by amplitude, at each frequency. Figure 5 shows an example measured oscilloscope data for Device A3 with corresponding fit. Table 3 summarizes the electrical performance of each device.

The existence of a signal component at the second harmonic corresponds to previously reported work [6] which was attributed to flexural stress maximums occurring in the actuation arms 2x during a single extensional cycle effectively doubling the frequency of the electrical readout. A similar nonlinear effect may be occurring in the $\omega_{o(\#1)}$ mode of this work.

The laser sensing results indicated that the mechanical frequency of self-sustained oscillation was indeed occurring at $\omega_{o(\#1)}$ for both devices. Figure 6 shows a representative dataset for Device A3 with LS fitting of the measured data to the expected 1D Lorentzian lineshape.

CONCLUSIONS AND FUTURE WORK

This work demonstrates thermal-piezoresistive self-sustained oscillators in the VHF regime. Unlike previous reported work at lower frequencies, evidence suggests the devices presented operate in a longitudinally symmetric flexural mode as opposed to the in-plane longitudinal
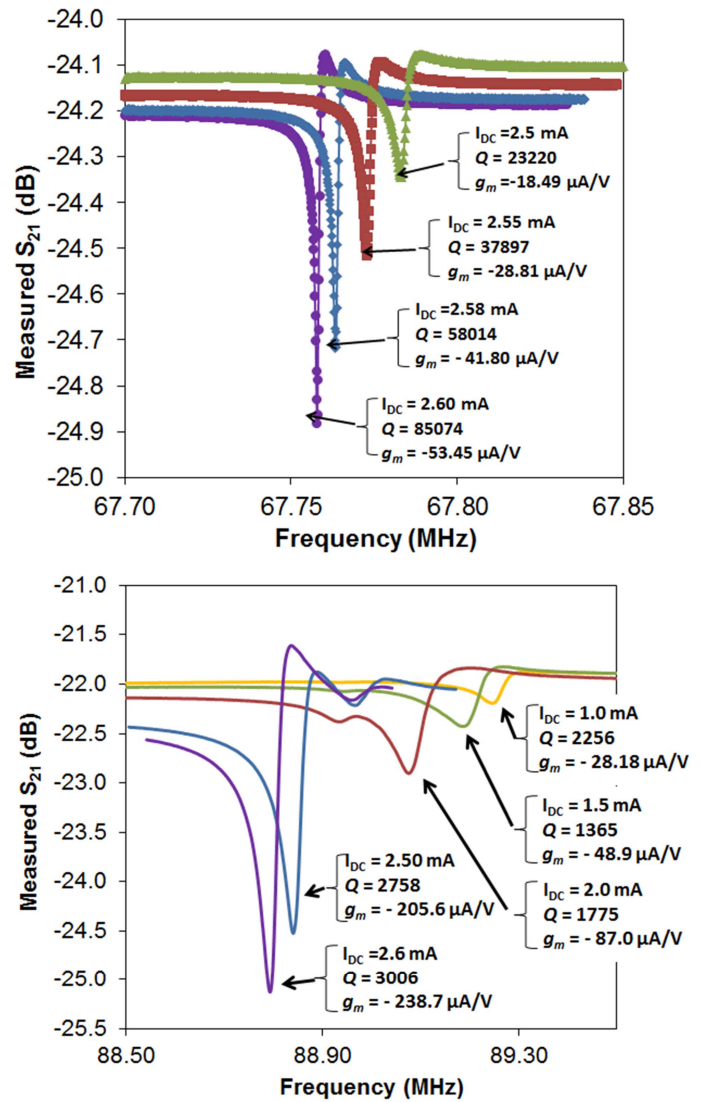

Figure 4: Measured $|S_{21}|$ data (ambient air) of Device C6 at $\omega_{o(\#1)}$ (Top) and $\omega_{o(\#2)}$ (Bottom) at different I_{DC} values with network analyzer power of -20dBm.

Table 3: Summary of Device Electrical Performance as Self-Sustained Oscillators

Device (R_dev)	Oscillator Current (mA)	Power (mW)	Pressure*	V_{p-pAC} (mV)	$f_{o\,\#(1)}$ (MHz)	$2f_{o\,(\#1)}$ (MHz)	% f_o	% $2f_o$
A3 (2.74 kΩ)	2.6	18.52	Vacuum	38.2	81.57	163.15	23.4	76.6
	3.117	26.61	Air	44.2	80.83	161.66	62.3	37.7
C6 (3.44 kΩ)	2.5	21.48	Vacuum	21.0	67.19	134.39	50.7	49.3
	2.7	25.06	Air	13.6	67.83	135.68	53.7	46.3

* Vacuum = 50-70 Torr, Air = Ambient air conditions in lab
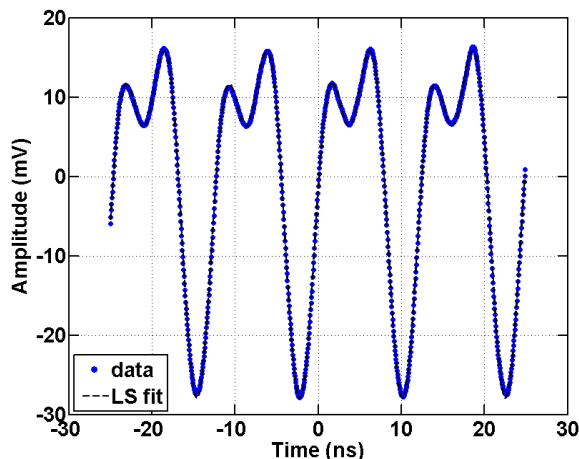
Figure 5: Device A3 measured oscilloscope data in ambient air with least squares (LS) fit I_{DC}=3.117mA with 62.3% content at 80.83MHz and 37.7% at 161.67MHz.
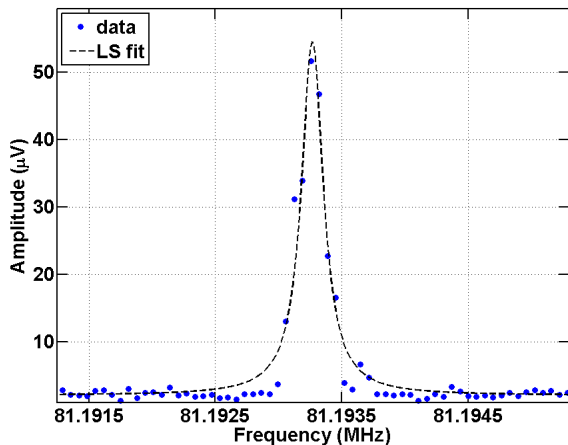

Figure 6: Measured laser detection output of spectrum analyzer for Device A3 at I_{DC} = 3.079mA with corresponding 1D Lorentzian fit.

mode they were intended for. Furthermore, while the mode of operation has a significantly higher *apparent Q*, attributed to self-Q enhancement, its g_m is small in comparison to the longitudinal mode.

This behavior raises the question, per (2), what makes the flexural mode preferable for self-sustained oscillation? One reason being considered is that the phase criteria needed for oscillation is being satiated with $\omega_{o(\#1)}$ but not $\omega_{o(\#2)}$. This explanation questions the validity of the lumped element model previously presented for these devices for use at these higher frequencies. Further work is being pursued along these lines.

REFERENCES

[1] A. Rahafrooz and S. Pourkamali, "Thermal-Piezoresistive Energy Pumps in Micromechanical Resonant Structures," *IEEE Transactions on Electron Devices*, vol. 59, no. 12, pp. 3587–3593, Dec. 2012.

[2] P. G. Steeneken, K. Le Phan, M. J. Goossens, G. E. J. Koops, G. J. A. M. Brom, C. van der Avoort, and J. T. M. van Beek, "Piezoresistive heat engine and refrigerator," *Nature Physics*, vol. 7, no. 4, pp. 354–359, Jan. 2011.

[3] H. J. Hall, A. Rahafrooz, J. J. Brown, V. M. Bright, and S. Pourkamali, "I-shaped thermally actuated VHF resonators with submicron components," *Sensors and Actuators A: Physical*, pp. 6–12, Dec. 2012.

[4] A. Rahafrooz and S. Pourkamali, "High-Frequency Thermally Actuated Electromechanical Resonators With Piezoresistive Readout," *IEEE Transactions on Electron Devices*, vol. 58, no. 4, pp. 1205–1214, 2011.

[5] A. Rahafrooz and S. Pourkamali, "Zero Bias Operation of Thermal-Piezoresistive Micromechanical Resonators via Internal Electromechanical Mixing," in *Hilton Head 2012 Proceedings*, 2012, pp. 375–378.

[6] A. Rahafrooz and S. Pourkamali, "High frequency dual-mode thermal-piezoresistive oscillators," in *2011 IEEE IFCS Proceedings*, 2011, pp. 1–4.

CONTACT

*H.J.Hall, tel: +1-303-492-7151;
Harris.Hall@colorado.edu